Chemistry–A European Journal
Research Article
doi.org/10.1002/chem.202200334
Chemistry Europe
European Chemical Societies Publishing
www.chemeurj.org

Metal-Organic Framework (MOF) Morphology Control by Design

Kuthuru Suresh,[a] Andre P. Kalenak,[a] Ania Sotuyo,[a] and Adam J. Matzger*[a, b]

Abstract: Exerting morphological control over metal-organic frameworks (MOFs) is critical for determining their catalytic performance and to optimize their packing behavior in areas from separations to fuel gas storage. A mechanism-based approach to tailor the morphology of MOFs is introduced and experimentally demonstrated for five cubic Zn_4O-based MOFs. This methodology provides three key features: 1) computational screening for selection of appropriate additives to change crystal morphology based on knowledge of the crystal structure alone; 2) use of additive to metal cluster geometric relationships to achieve morphologies expressing desired crystallographic facets; 3) potential for suppression of interpenetration for certain phases.

Introduction

The morphology of a crystal is the result of internal (crystal structure and crystal lattice defects) and external (growth solvent, level of supersaturation, presence of impurities, time, temperature, etc.) factors that impact the relative growth rates of crystal facets.[1] The basic principle guiding external appearance is that the facets which grow most slowly are those expressed on the crystal surface. Engineering of particle/crystal morphology is one of the central tasks of nanoscience and catalysis. Controlling morphology and increasing external surface area of specific crystal facets principally determine their catalytic activity by supporting various active sites that affect the chemical reaction barriers.[2–6] For example, metal-organic frameworks (MOFs) with expressing different crystal facets show face-selective catalysis;[7–10] ZIF-67 and ZIF-68 MOFs particles with a {002} facet exhibit greater catalytic performance than particles with {011} and {111} facets.[7] Similarly, distinctly different catalytic activity between different crystal facets of NENU-3a has been reported.[10] In that study, cubic crystal morphology (six {100} facets) samples exhibit better catalytic performance than crystals with an octahedral morphology (eight {111} facets).[10] Typically, MOF crystal morphology control studies include additives and/or altering the pH of the growth medium, and organic linker functionalization.[7–19] For instance, metal coordinating polymers have been used as additives to inhibit crystal growth along selected crystallographic directions and control MOF morphology.[14,15] In analogy to inorganic nanoparticles,[20,21] surfactants have also been used to generate new morphologies of MOFs.[11,13,16] Recently, we reported the generation of new non-cubic morphologies by employing various polycarboxylic acids as additives for MOF-5.[22] Non-cubic morphologies of MOF-5 display superior packing densities and compaction properties, relative to cubic crystals, allowing optimization of volumetric gas storage density and attainment of bed packing densities approaching single crystal values with minimal gravimetric storage penalty[22] To date, no generally applicable strategy exists for MOF morphology engineering, and there is insufficient fundamental understanding of how to direct the formation of crystals with defined morphologies; selection of suitable additives for habit modification and controlling the crystallization of a MOF is generally an empirical pursuit leading to an inability to exert purposeful control.

In the present study, we demonstrate a rational design strategy to engineer MOF crystal morphology through additive design. Aromatic dicarboxylic acids were selected as additives that can coordinate to two metal clusters of a MOF situated diagonally across a pore window, resulting in facially-selective suppression of growth rates of crystal facets thus yielding new morphologies (Scheme 1) without changing the original phase. In brief, the approach begins with an analysis of the pore system of the MOF from the crystal structure and designs a suitable additive based on the measured distances between two diagonally situated clusters across a pore window. This additive design strategy can be generally applied to synthesize new MOF morphologies.

[a] *Dr. K. Suresh, A. P. Kalenak, Dr. A. Sotuyo, Prof. A. J. Matzger*
Department of Chemistry
University of Michigan
930 North University Avenue, Ann Arbor, MI48109-1055 (United States)
E-mail: matzger@umich.edu

[b] *Prof. A. J. Matzger*
Macromolecular Science and Engineering Program
University of Michigan
930 North University Avenue, Ann Arbor, MI48109-1055 (United States)

Supporting information for this article is available on the WWW under https://doi.org/10.1002/chem.202200334

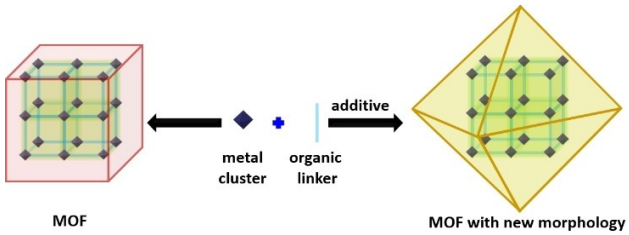

Scheme 1. Schematic of MOF synthesis with and without the presence of an additive. A change in relative crystal growth rates of crystal facets due to the presence of the additive results in altered crystal morphology without changing the underlying crystal structure.

Results and Discussion

To develop a general methodology for controlled production of new MOF morphologies, a series of crystallographically cubic Zn_4O-based MOFs were selected: $Zn_4O(FMA)_3$, MOF-5, IRMOF-3, SNU-70, and IRMOF-8. Each MOF typically possesses a cubic morphology with six {100} facets expressed. From a structural standpoint, each MOF has an oxide-centered Zn_4O tetrahedron that is edge-connected by six approximately linear carboxylates (FMA = fumarate, MOF-5 = terephthalate, IRMOF-3 = 2-aminoterephthalate, SNU-70 = 4-carboxylate-cinnamate, IRMOF-8 = 2,6-naphthalene dicarboxylate) to give the octahedron-shaped secondary building unit that extends into a three-dimensional cubic porous network.[23–26] However, these MOFs differ in carboxylate linker length or functional group and have cubic pores of varying size. The measured oxo-oxo separation of two Zn_4O clusters that are positioned diagonally across a pore window in the {100} plane are 15.30 Å ($Zn_4O(FMA)_3$), 18.30 Å (MOF-5), 18.21 Å (IRMOF-3), 21.38 Å (SNU-70), and 21.28 Å (IRMOF-8). The measured C to C distance across a pore window in the {100} plane of selected MOFs (between carboxylates, highlighted in blue in Figure 1a–d) are 10.12 Å ($Zn_4O(FMA)_3$,13.24 Å (MOF-5), 13.21 Å (IRMOF-3), 16.50 Å (SNU-70), and 16.28 Å (IRMOF-8). One key point to consider when designing appropriate additives that serve as MOF morphology modifiers is that linear carboxylic acid additives may result in new phases incorporating zinc and two different carboxylic acid linkers.[27] Non-linear (bent) dicarboxylic acid molecules are less prone to this behaviour and provide a more ideal geometry for cluster approach. Additionally, a second key point is that the C to C distance of the additive needs to approximately match the measured C to C distance of two carboxylates attached to diagonally opposed metal clusters, so that the additive can favor bridging two metal clusters across a pore window during crystal growth. Accordingly, an array of bent aromatic dicarboxylic acids were chosen as additives: isophthalic acid, biphenyl-3,4′-dicarboxylic acid, *m*-terphenyl-4,4′-dicarboxylic acid, and *m*-quaterphenyl-4,4′-dicarboxylic acid. Theoretical calculations were performed to select an appropriate additive for the selected MOFs; the predicted C to C distances for this series of additives are 5.02 Å (isophthalic acid), 8.98 Å (biphenyl-3,4′-dicarboxylic acid), 12.43 Å (*m*-terphenyl-4,4′-dicarboxylic acid), 16.37 Å and (*m*-quaterphenyl-4,4′-dicarboxylic acid). From these theoretical calculations, the biphenyl-3,4′-dicarboxylic acid C to C distance of 8.98 Å is closest to two diagonal metal cluster C to C spacing of $Zn_4O(FMA)_3$ (10.12 Å) whereas the *m*-terphenyl-4,4′-dicarboxylic acid C to C distance of 12.43 Å is closer to two diagonal metal cluster C to C spacings of MOF-5 (13.24 Å) and

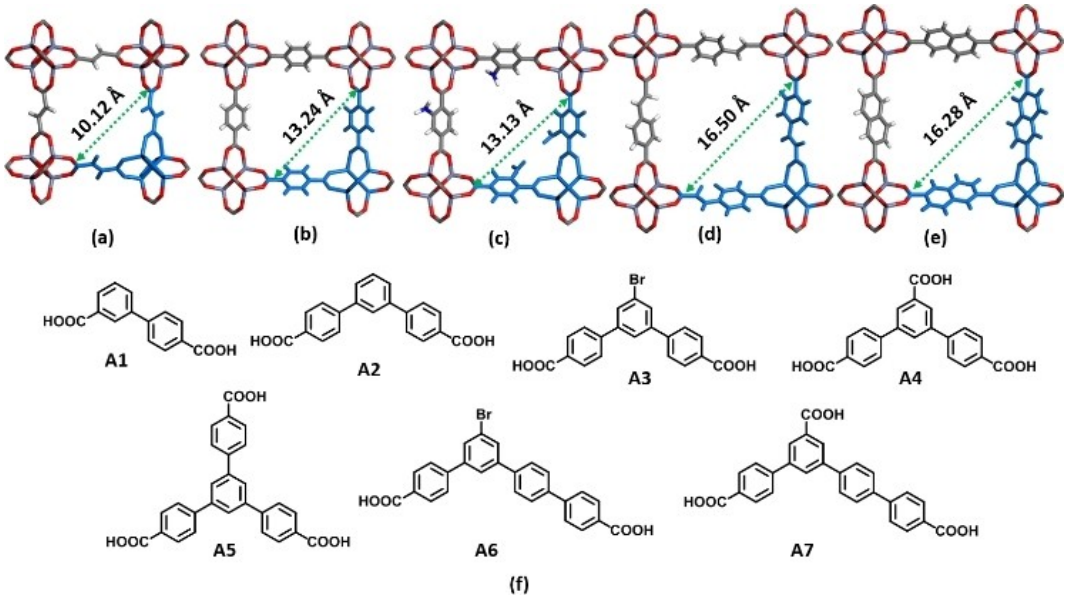

Figure 1. The structure of the pore window in the {100} plane of $Zn_4O(FMA)_3$ (a), MOF-5 (b), IRMOF-3 (c), SNU-70 (d), and IRMOF-8 (e). The C to C distances of the MOF two diagonal clusters are highlighted in blue. (f) Molecular structures of designed additives used for this study: A1 = biphenyl-3,4′-dicarboxylic acid, A2 = *m*-terphenyl-4,4′-dicarboxylic acid, A3 = 5′-bromo-[1,1′:3′,1″-terphenyl]-4,4′-dicarboxylic acid, A4 = [1,1′:3′,1″-terphenyl]-4,4′,5′-tricarboxylic acid, A5 = 1,3,5-tris(4-carboxyphenyl)benzene, A6 = 5′-bromo-[1,1′:3′,1″:4″,1‴-quaterphenyl]-4,4‴-dicarboxylic acid, and A7 = [1,1′:3′,1″:4″,1‴-quaterphenyl]-4,4‴,5′-tricarboxylic acid.

IRMOF-3 (13.13 Å). For *m*-quaterphenyl-4,4′-dicarboxylic acid, a calculated C to C distance (16.37 Å) matches well to the C to C distance for both SNU-70 (16.50 Å) and IRMOF-8 (16.28 Å). Thus biphenyl-3,4′-dicarboxylic acid, *m*-terphenyl-4,4′-dicarboxylic acid, and *m*-quaterphenyl-4,4′-dicarboxylic acid and their functionalized derivatives (Figure 1e) were selected as suitable additives to synthesize new morphologies for the five selected MOFs because they can bridge two diagonal clusters in a MOF pore, regulating crystal growth and morphology of the final crystal. The addition of these selected additives were screened at various mol% level (~1 to 40 mol%) to obtain new controlled morphologies. From these screening experiments, additives in the lowest concentration that resulted in new controlled non-cubic morphologies, without changing the original phase, were employed.

$Zn_4O(FMA)_3$

Cubic morphology $Zn_4O(FMA)_3$ crystals[28] (Figure 2a) are synthesized solvothermally by mixing $Zn(NO_3)_2 \cdot 4H_2O$ and fumaric acid (H_2FMA) in N,N-diethylformamide (DEF) and heating the mixture to 100 °C in an oven for 24 h (See Experimental section, Supporting Information). As predicted to obtain controlled non-cubic morphology crystals of $Zn_4O(FMA)_3$, biphenyl-3,4′-dicarboxylic acid (A1) is an appropriate additive. The addition of A1 (~22 mol%) to the initial reagents mixture of $Zn_4O(FMA)_3$ and heating at 100 °C for 24 h yielded non-cubic, truncated octahedral morphology ($Zn_4O(FMA)_3$-tO_h(A1), Figure 2a) crystals with eight hexagonal {110} and six square {100} crystal facets.

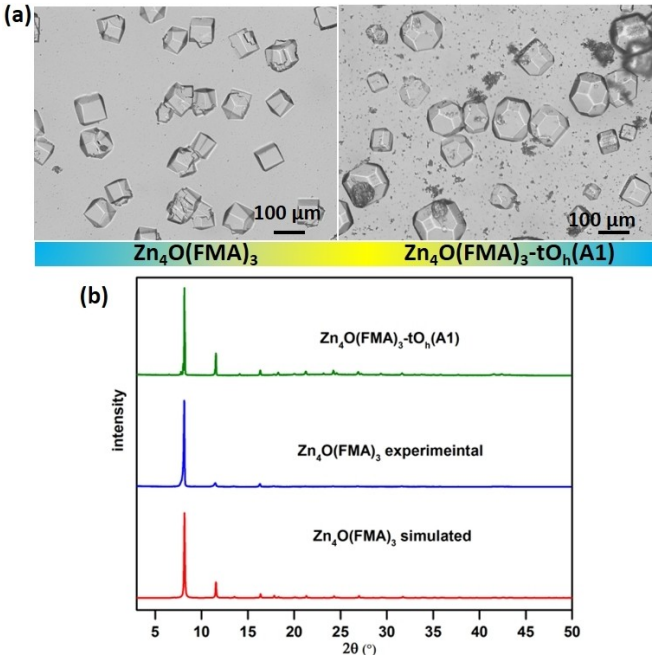

Figure 2. (a) Optical images of cubic and truncated octahedral morphologies of $Zn_4O(FMA)_3$. (b) PXRD pattern of truncated octahedral morphology sample compared with the simulated pattern of $Zn_4O(FMA)_3$ computed from its crystal structure (CSD refcode XOZXOA).

PXRD of the obtained $Zn_4O(FMA)_3$-tO_h(A1) is consistent with the simulated pattern of $Zn_4O(FMA)_3$ extracted from the single crystal X-ray structure (Figure 2b) indicating no change in phase. The crystal size distributions and statistics for $Zn_4O(FMA)_3$ and $Zn_4O(FMA)_3$-tO_h(A1) are represented in Supporting Information (Figure S5 and Table S1). Proton NMR analysis of $Zn_4O(FMA)_3$-tO_h(A1) crystals after digestion in DCl/DMSO-d_6 solution reveals that less than 2 mol% of A1 is incorporated (Figure S7, Supporting Information). This additive does not yield a new phase, as confirmed through PXRD (Figure 2b); the small amount of A1 may occupy defect sites but likely exerts morphology control by reversibly binding the {110} face during growth. BET surface area analysis of the $Zn_4O(FMA)_3$-tO_h(A1) morphology sample demonstrates that there is no significant reduction in BET surface area (2017 m^2/g for $Zn_4O(FMA)_3$-tO_h(A1)) compared to optimal cubic crystals surface area (2009 m^2/g for $Zn_4O(FMA)_3$).[29]

MOF-5 and IRMOF-3

Solvothermal synthesis (DEF, 100 °C for 16–24 h) of MOF-5 and IRMOF-3 without additives generates cubic morphology crystals. Non-cubic morphology crystals were obtained by addition of the additive *m*-terphenyl-4,4′-dicarboxylic acid (A2) and its functionalized derivatives ((5′-bromo-[1,1′:3′,1″-terphenyl]-4,4′-dicarboxylic acid (A3), [1,1′:3′,1″-terphenyl]-4,4′,5′-tricarboxylic acid (A4), and 1,3,5-tris(4-carboxyphenyl)benzene (A5)). Solvothermal synthesis was carried out by mixing $Zn(NO_3)_2 \cdot 4H_2O$, organic linker (H_2BDC/H_2-BDC-NH_2), and additive (A2/A3/A4/A5) at various mol% levels in DEF and heating the mixture to 100 °C in an oven for 16–24 h (See Experimental section, Supporting Information). These synthesis conditions readily yield non-cubic morphology crystals for both MOF-5 and IRMOF-3 (Figure 3a and b) and their crystal size distributions and statistics are represented in Supporiting Information (Figure S9 and S16 and Table S2 and S3). In the case of MOF-5, the addition of A2 (~30 mol%) or A3(~25 mol%) or A4 (~6 mol%) to the initial MOF-5 reagent mixture generated crystals with uniform rhombic dodecahedral (R_d) morphology expressing twelve equilateral rhombic {110} crystal facets (MOF-5-R_d(A2), MOF-5-R_d(A3), and MOF-5-R_d (A4)). When the A5 (~4 mol%) additive was added to the MOF-5 reaction mixture, the result was a uniform octahedral (O_h) morphology crystals with eight equilateral triangular {111} crystal facets (MOF-5-O_h(A5)).[23,29,30] Similarly in IRMOF-3, A2 (~31 mol%) or A4 (~9 mol%) added to the initial IRMOF-3 reagent mixture generated truncated octahedral (tO_h) morphology crystals with eight hexagonal {110} and six square {100} crystal facets (IRMOF-3-tO_h(A3) and IRMOF-3-tO_h(A4)). The addition of A3 (~27 mol%) generated crystals with uniform rhombic dodecahedral (R_d) morphology (IRMOF-3-R_d(A3)), whereas A5 (~3 mol%) yielded uniform octahedral (O_h) morphology crystals with eight equilateral triangular {111} crystal facets (IRMOF-3-O_h(A5)). PXRD patterns of the obtained new non-cubic morphologies for both MOFs are consistent with their simulated patterns extracted from single crystal X-ray structures (Figure 3c and d), and NMR analysis determined that

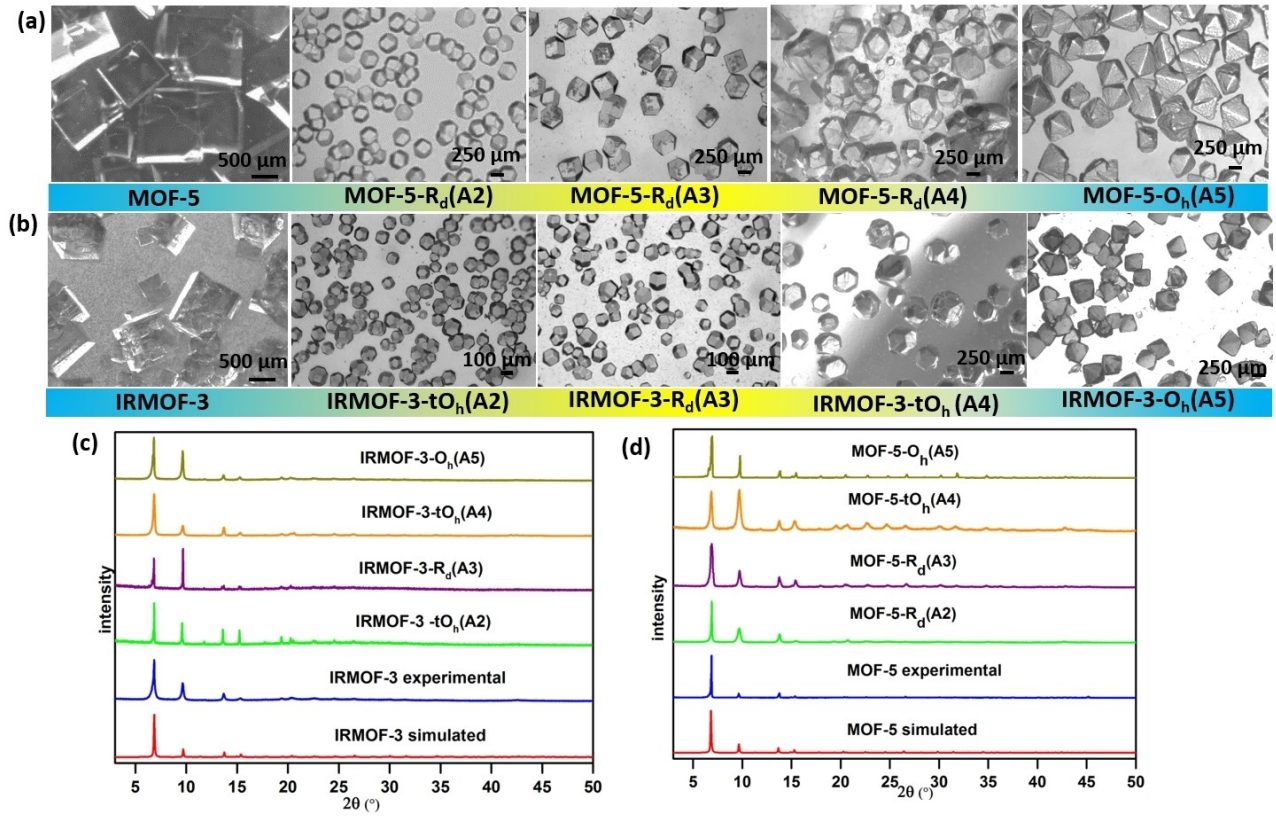

Figure 3. (a) and (b). Optical images of cubic and non-cubic morphologies of MOF-5 and IRMOF-3. (c) and (d) PXRD patterns of new morphologies of MOF-5 and IRMOF-3 compared with the simulated patterns of MOF-5 and IRMOF-3 computed from their crystal structures (CSD refcode SAHYOQ (MOF-5) and EDUSUR).

less than 1 mol% additive incorporation takes place (see in Supporting Information). BET analysis of MOF-5-R_d(A2) and IRMOF-3-tO_h(A2) morphology samples determined that there is no significant reduction in surface area (3355 m^2/g for MOF-5-R_d(A2) and 2646 m^2/g for IRMOF-3-tO_h(A2)) compared to their optimal cubic surface area (3505 m^2/g for MOF-5[21] and 2777 m^2/g for IRMOF-3[31]).

SNU-70 and IRMOF-8

SNU-70 and IRMOF-8 are isomorphous MOFs and, as expected from theoretical predictions, *m*-quarterphenyl-4,4′-dicarboxylic acid led to new morphologies. Thus, two functionalized *m*-quaterphenyl-4,4′-dicarboxylic acid derivatives (A6 (5′-bromo-[1,1′:3′,1″:4″,1‴-quaterphenyl]-4,4‴-dicarboxylic acid) and A7 ([1,1′:3′,1″:4″,1‴-quaterphenyl]-4,4‴,5′-tricarboxylic acid)) were used as additives for morphology control. Cubic crystals of SNU-70 formed upon heating the MOF reagents at 100 °C for 18 h in the absence of the additive (Figure 4a). The addition of A6 (~7 mol%) and A7 (~7 mol%) to the initial reagent mixture of SNU-70 and heating at 100 °C for 18 h yielded crystals with rhombic dodecahedral morphology (SNU-70-R_d(A6) and SNU-70-R_d(A7), Figure 4a) and their crystal size distributions and statistics are represented in Suppoting Information (Figure S23 and Table S4). The addition of A7 (~9 mol%) to the initial SNU-70 reagent mixture generated truncated octahedral (tO_h) morphology crystals (SNU-70-tO_h(A7). PXRD patterns of the newly obtained morphology samples match unmodified SNU-70 (Figure 4d). Digestion of each of these in DCl/DMSO-d_6 solution reveals that less than 1 mol% of additive is incorporated. BET analysis of SNU-70-R_d(A7) and SNU-70-tO_h(A7) morphology samples determined that there is very minor reduction in surface area (4732 m^2/g for SNU-70-R_d(A7) and 4864 m^2/g for SNU-70-tO_h(A7)) compared to optimal cubic crystal surface area (4944 m^2/g).[30] It has been reported that the IRMOF-8 synthesis at room temperature and solvothermal conditions leads to interpenetrated and non-interpenetrated MOFs, respectively.[32] Mixing the MOF reagents and then allowing the mixture to sit at room temperature for eight days generated mixed cubic and cuboctahedral morphology crystals (Figure 4b). However, with A6 or A7 (~11 mol%) additives in the initial IRMOF-8 reagents mixture, a new rhombic dodecahedral morphology was observed after twelve days (IRMOF-8-RT-R_d(A6) and IRMOF-8-RT-R_d(A7), Figure 4b). At elevated temperatures, the addition of A6 (~11 mol%) and A7 (~11 mol%) additives to the IRMOF-8 reagent mixture (heated at 85 °C for 24 h) generates crystals with a new uniform rhombic dodecahedral morphology (IRMOF-8-HT-R_d(A6) and IRMOF-8-HT-R_d(A7), Figure 4c) and their crystal size distributions and statistics are

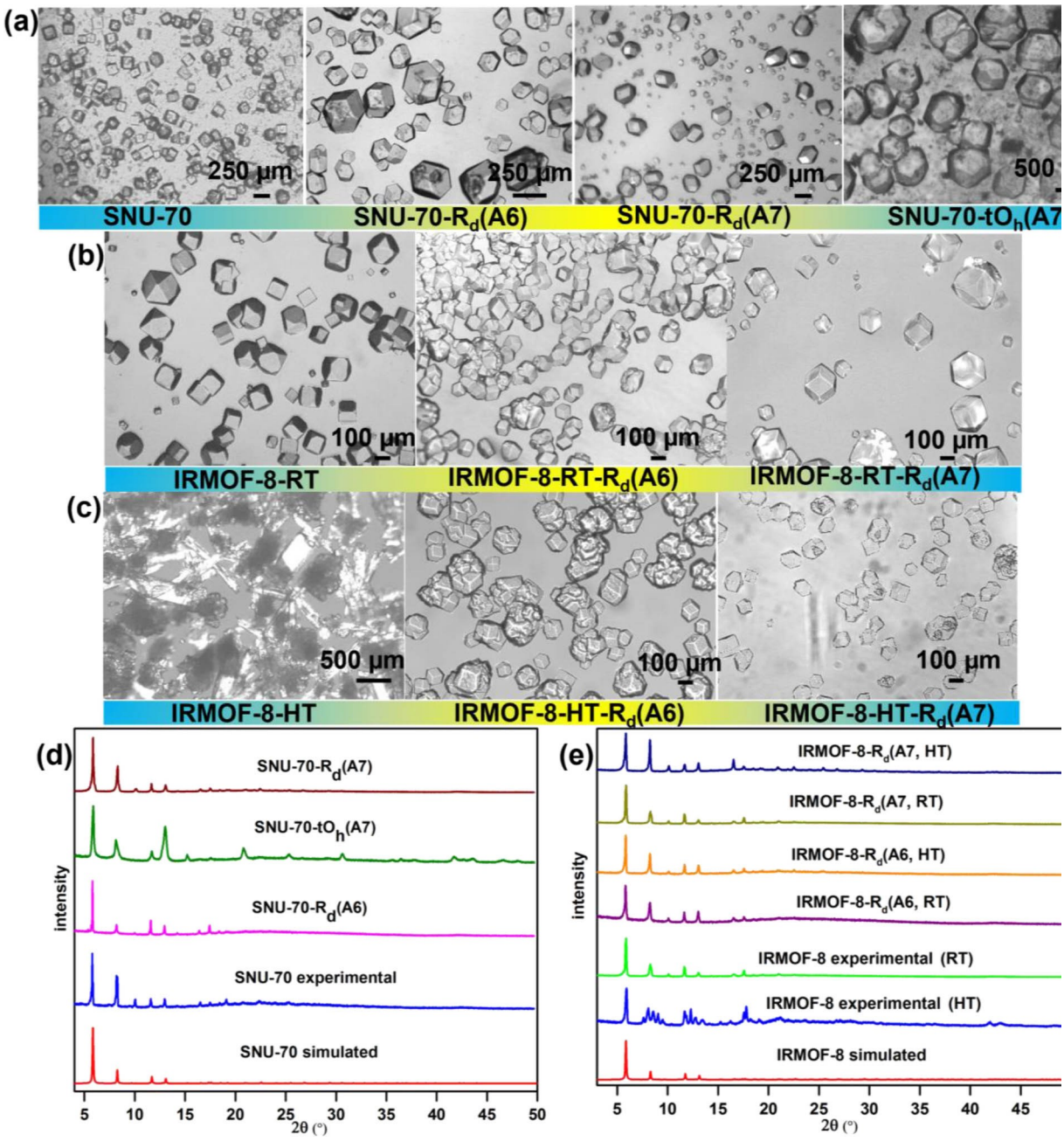

Figure 4. (a), (b), and (c). Optical images of cubic and non-cubic morphologies SNU-70 and IRMOF-8. (d) and (e). PXRD patterns of new morphologies of SNU-70 and IRMOF-8 compared with simulated patterns of SNU-70 and IRMOF-8 computed from their crystal structures (CSD refcode GEBPEK and EDUTUS).

represented in Supporting Information (Figure S29 and Table S5). PXRD patterns of these newly obtained morphology samples demonstrate that they are non-interpenetrated IRMOF-8 (Figure 4e). Digestion of IRMOF-8-HT-R_d(A6) and IRMOF-8-HT-R_d(A7) morphologies in DCl/DMSO-d_6 solution demonstrates that incorporated final mol% additive as with the other MOFs. BET analysis of the IRMOF-8-RT-R_d(A6) and IRMOF-8-HT-R_d(A6) morphology samples demonstrates that there is no significant reduction in surface area (4663 m^2/g for IRMOF-8-RT-R_d(A6) and 4455 m^2/g for IRMOF-8-HT-R_d(A6)). Specifically, IRMOF-8-RT-R_d-(A6) shows slightly higher surface value when compared to reported optimal cubic crystal surface area (4461 m^2/g for IRMOF-8-RT).[33] This IRMOF-8 new morphology synthesis using additives at elevated temperatures selectively yields exclusively the non-interpenetrated phase of IRMOF-8. We hypothesize that the additive is responsible for the IRMOF-8 non-interpenetrated phase formation because it can coordinate between two Zn_4O clusters situated diagonally across a pore window in the {100} plane of IRMOF-8 during phase formation, which effectively suppresses the formation of an interpenetrated framework with new controlled morphology. In this process, the additive acts as an "interpenetrated phase suppressor". This

mechanism is distinguished from interpenetration suppression strategies where multiple linkers are incorporated into a single MOF[27] because the suppressor acts transiently in the present case and thus does not change the overall MOF structure.

Additives which did not match the carboxylate C to C bond distance for any selected MOF and bulky monocarboxylic acids resulted in no change in cubic morphology. For instance, the addition of isophthalic acid, *m*-terphenyl-4,4′-dicarboxylic acid, and 5′-bromo-[1,1′:3′,1″:4″,1‴-quaterphenyl]-4,4‴-dicarboxylic acid at 10–50 mol% level into the initial $Zn_4O(FMA)_3$ MOF reagent mixture resulted in cubic crystal morphology. These results are also mirrored in other MOFs (MOF-5, IRMOF-3, SNU-70 and IRMOF-8) in the presence of C to C distance mismatched additives in the initial MOF reagent mixture. This clearly demonstrates that additives that are larger or smaller than the cluster spacing of MOF in the crystal structure do not yield new morphologies.

In situ MOF crystal growth monitoring

Furthermore, to monitor in situ MOF crystallization in the presence of an additive, MOF-5-R_d(A3) was selected. The reaction between $Zn(NO_3)_2 \cdot 4H_2O$ and H_2BDC in DEF in the presence of 25 mol% A3 additive at 100 °C for 24 h was monitored (see experimental and instrumental details in Supporting Information). Figure S34 shows different stages of the MOF growth under isothermal conditions. The appearance of MOF crystals at 12 h corresponds closely to the induction time for this system, whereas the time at which the crystals stop growing in size (18 h) corresponds to complete MOF crystallization. This crystallization process results in uniform rhombic dodecahedral morphology crystals. Additionally, no morphological transitions were observed during the course of the reaction.

Engineering of crystal morphology mechanism

The ultimate morphology of a crystal depends on the growth rates of the different crystallographic facets. Slow growing facets have the most influence on crystal morphology whereas fast-growing facets may have little to no effect on the morphology of a crystal. The growth rate of a crystal facet is governed by the crystal structure, defects, and the crystallization conditions. We propose a mechanism to explain morphological changes in cubic MOFs in Scheme 2 (this mechanism is described with MOF-5 as an example). It was observed that synthesis of $Zn_4O(FMA)_3$, MOF-5, IRMOF-3, and SNU-70 in the absence of the additives consistently resulted in cubic morphology crystals with six {100} crystallographic facets. This indicates that the slowest rate of crystal growth occurs along the {100} crystallographic facet direction (Scheme 2a). In the case of IRMOF-8 without additives, mixed cubic (six {100} facets) and cuboctahedral (six {100} and eight {111} facets) morphologies occur due to slow growth rates of {100} and {111} facets at room temperature.

In the presence of various additives, crystal morphologies of octahedral (eight equilateral triangular {111} facets), rhombic dodecahedral (twelve rhombic {110} facets), and truncated octahedral (six square {100} and eight rhombic {110} facets) morphologies were obtained. To induce this morphological change, we propose that during crystal growth if the additive blocks MOF growth along a specific crystallographic facet direction, it will slow the growth rate of this facet and lead to expression on the crystal surface. Bridging two diagonally disposed Zn_4O clusters in a {100} pore window along the {110} facet direction through dicarboxylate additives (A1, A2, A3, A4, A6, and A7) favors {110} crystallographic facet expression. Depending on the MOF-dicarboxylate additive combination this leads to {110} facets having competative growth rates with {100} facets, leading to truncated octahedral morphology (Scheme 2b), or complete suppression of {100} facets leading to rhomonic dodecahedral morphology (Scheme 2c). By contrast, the tricarboxylate additive (A5 in MOF-5-O_h(A5) and IRMOF-3-O_h(A5)) blocks growth along the {111} facet direction through three Zn_4O cluster connections in a pore by promoting the expression of {111} facets on the crystal surface at the expense of all regularly observed {100} facets. Therefore, octahedral morphology crystals are observed (Scheme 2d). These results clearly show that the design and synthesis of morphologies with desired crystallographic facets can be achieved based on an understanding and use of connections between additives and metal cluster. By contrast, additives that exhibit C to C distances larger or smaller than cluster spacing in a pore window of MOFs and bulky monocarboxylic acids do not yield new morphologies. A few morphologies exhibit larger crystal sizes due to inhibition of nucleation in presence of additives. Additionally, the enhanced molar ratio of metal salt and organic linker when compared to their parent MOFs molar ratio yielded morphologies with larger crystal sizes ($Zn_4O(FMA)_3$-tO_h(A1) and SNU-70-tO_h(A7)).

Conclusions

MOF morphology engineering has lacked mechanism-based design approaches, thus hindering the development of methods for the production of MOFs with controlled morphologies. In the present study, Zn_4O cluster-based MOFs of multiple morphologies are achieved with designed additives in the initial MOF reagent mixture without changing the original phase. Computation allows for selection of appropriate additives to change crystal morphology based on knowledge of the crystal structure. BET surface area analysis of activated new MOF morphology samples demonstrate preservation of internal surface area. An additional significant finding is that the additive can also act as an "interpenetrated phase suppressor" (e.g., to give exclusively non-interpenetrated phase of IRMOF-8 at elevated temperature conditions). Additionally, plausible relative crystal growth rates of different morphologies of the MOFs have been proposed, which demonstrate how the use of additive metal cluster connections leads to morphologies with desired crystallographic facets. Broadly, findings from of our

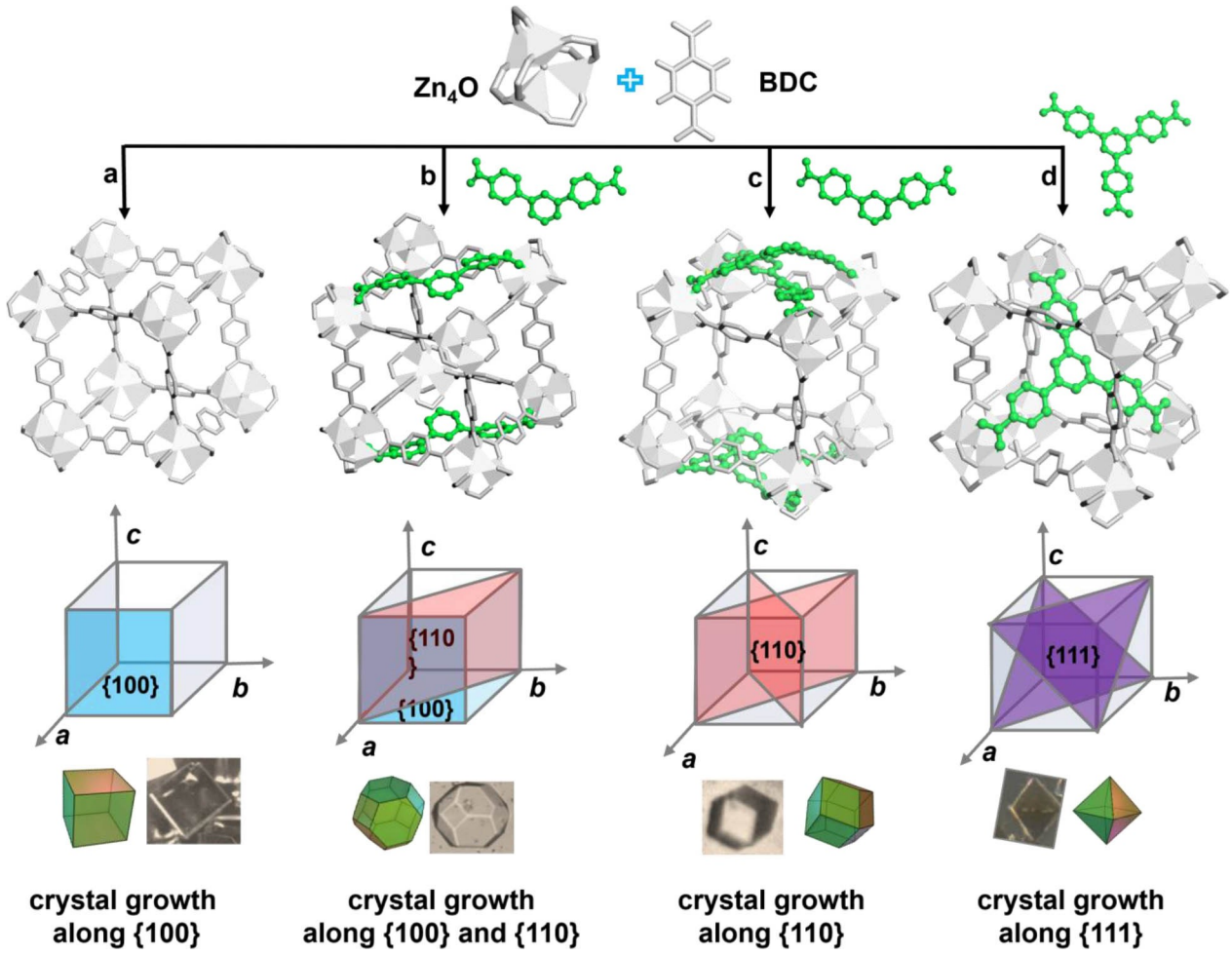

Scheme 2. A schematic of crystal growth mechanism for cubic and non-cubic morphologies of the MOF. The cubic crystal morphology (a) is controlled by the slower crystal growth along {100} facet direction. The additive blocks MOF growth along {110} or {111} crystallographic facet directions partially or at the expense of all {100} facets during crystal growth which results in the formation of rhombic dodecahedral (b), truncated octahedral (c), and octahedral (d) crystal morphologies.

approach combines the selection of additives through the computational design and synthesis of MOF new crystal morphologies while maintaining internal surface area (minimal to no pore blockage) represents a generalizable strategy for achieving face-selective catalysis and high material packing density to increase volumetric gas storage.

Acknowledgements

The authors acknowledge the financial support for this study was provided by the US Department of Energy-BES Grant. no. DE-SC0004888.

Conflict of Interest

The authors declare no conflict of interest.

Data Availability Statement

The data that support the findings of this study are available in the supplementary material of this article.

Keywords: additive · crystal growth rate · crystal morphology · metal-organic framework (MOF) · morphology engineering

[1] R. J. Davey, S. L. M. Schroeder, J. H. ter Horst, *Angew. Chem. Int. Ed.* **2013**, *52*, 2166–2179; *Angew. Chem.* **2013**, *125*, 2220–2234.
[2] M. Shi, G. Li, J. Li, X. Jin, X. Tao, B. Zeng, E. A. Pidko, R. Li, C. Li, *Angew. Chem. Int. Ed.* **2020**, *59*, 6590–6595; *Angew. Chem.* **2020**, *132*, 6652–6657.
[3] S. Wang, G. Liu, L. Wang, *Chem. Rev.* **2019**, *119*, 5192–5247.
[4] G. Wang, Z. Yang, Y. Du, Y. Yang, *Angew. Chem. Int. Ed.* **2019**, *58*, 15848–15854; *Angew. Chem.* **2019**, *131*, 15995–16001.
[5] P. Strasser, M. Gliech, S. Kuehl, T. Moeller, *Chem. Soc. Rev.* **2018**, *47*, 715–735.
[6] R. A. Schoonheydt, *Angew. Chem. Int. Ed.* **2008**, *47*, 9188–9191; *Angew. Chem.* **2008**, *120*, 9328–9331.
[7] J. Wan, D. Liu, H. Xiao, H. Rong, S. Guan, F. Xie, D. Wang, Y. Li, *Chem. Commun.* **2020**, *56*, 4316–4319.

[8] M. B. J. Roeffaers, B. F. Sels, H. Uji-i, B. Blanpain, P. L. ′hoëst, P. A. Jacobs, F. C. D. Schryver, J. Hofkens, D. E. De Vos, *Angew. Chem. Int. Ed.* **2007**, *46*, 1706–1709; *Angew. Chem.* **2007**, *119*, 1736–1739.
[9] M. B. J. Roeffaers, R. Ameloot, M. Baruah, H. Uji-I, M. Bulut, G. De Cremer, U. Müller, P. A. Jacobs, J. Hofkens, B. F. Sels, D. E. De Vos, *J. Am. Chem. Soc.* **2008**, *130*, 5763–5772.
[10] Y. Liu, S. Liu, D. He, N. Li, Y. Ji, Z. Zheng, F. Luo, S. Liu, Z. Shi, C. Hu, *J. Am. Chem. Soc.* **2015**, *137*, 12697–12703.
[11] A. Umemura, S. Diring, S. Furukawa, H. Uehara, T. Tsuruoka, S. Kitagawa, *J. Am. Chem. Soc.* **2011**, *133*, 15506–15513.
[12] K. A. Colwell, M. N. Jackson, R. M. Torres-Gavosto, S. Jawahery, B. Vlaisavljevich, J. M. Falkowski, B. Smit, S. C. Weston, J. R. Long, *J. Am. Chem. Soc.* **2021**, 143, 13, 5044–5052.
[13] M. Pang, A. J. Cairns, Y. Liu, Y. Belmabkhout, H. Chun Zeng, M. Eddaoudi, *J. Am. Chem. Soc.* **2012**, *134*, 13176–13719.
[14] T.-H. Chen, L. Wang, J. V. Trueblood, V. H. Grassian, S. M. Cohen, *J. Am. Chem. Soc.* **2016**, *138*, 9646–9654.
[15] S. Ayala Jr, K. C. Bentz, S. M. Cohen, *Chem. Sci.* **2019**, *10*, 1746–1753.
[16] S. Alizadeh, D. Nematollahi, *J. Am. Chem. Soc.* **2017**, *139*, 4753–4761.
[17] C. R. Marshall, S. A. Staudhammer, C. K. Brozek, *Chem. Sci.* **2019**, *10*, 9396–9408.
[18] C. R. Marshall, E. E. Timmel, S. A. Staudhammer, C. K. Brozek, *Chem. Sci.* **2020**, *11*, 11539–11547.
[19] C. A. Allen, S. M. Cohen, *Inorg. Chem.* **2014**, *53*, 7014–7019.
[20] L. Huang, X. Zhang, Q. Wang, Y. Han, Y. Fang, S. Dong, *J. Am. Chem. Soc.* **2018**, *140*, 1142–1147.
[21] T. Song, F. Gao, S. Guo, Y. Zhang, S. Li, H. You, Y. Du, *Nanoscale* **2021**, *13*, 3895–3910.
[22] K. Suresh, D. Aulakh, J. Purewal, D. J. Siegel, M. Veenstra, A. J. Matzger, *J. Am. Chem. Soc.* **2021**, *143*, 28, 10727–10734.
[23] M. Xue, Y. Liu, R. M. Schaffino, S. Xiang, X. Zhao, G.-S. Zhu, S.-L. Qiu, B. Chen, *Inorg. Chem.* **2009**, *48*, 11, 4649–4651.
[24] H. Li, M. Eddaoudi, M. O′Keeffe, O. M. Yaghi, *Nature* **1999**, *402*, 276–279.
[25] M. Eddaoudi, J. Kim, N. Rosi, D. Vodak, J. Wachter, M. O′Keeffe, O. M. Yaghi, *Science* **2002**, *295*(5554), 469–472.
[26] T. K. Prasad, M. P. Suh, *Chem. Eur. J.* **2012**,*18*(28), 8673–8680.
[27] K. Koh, J. D. Van Oosterhout, S. Roy, A. G. Wong-Foy, A. J. Matzger, *Chem. Sci.* **2012**, *3* (8), 2429–2432.
[28] P. Guo, D. Dutta, A. G. Wong-Foy, D. W. Gidley, A. J. Matzger, *J. Am. Chem. Soc.* **2015**, *137*, 2651–2657.
[29] K. Koh, A. G. Wong-Foy, A. J. Matzger, *Angew. Chem. Int. Ed.* **2008**, *47*, 677–680; *Angew. Chem.* **2008**, *120*, 689–692.
[30] T.-H. Park, A. J. Hickman, K. Koh, S. Martin, A. G. Wong-Foy, M. S. Sanford, A. J. Matzger, *J. Am. Chem. Soc.* **2011**, *133*(50), 20138–20141.
[31] R. A. Dodson, A. J. Matzger, *ACS Materials Lett.* **2019**, *1*, 344–349.
[32] A. Ahmed, S. Seth, J. Purewal, A. G. Wong-Foy, M. Veenstra, A. J. Matzger, D. J. Siegel, *Nat. Commun.* **2019**, *10* (1), 1568(1–9).
[33] J. I. Feldblyum, A. G. Wong-Foy, A. J. Matzger, *Chem. Commun.* **2012**, *48*, 9828–9830.

Manuscript received: February 2, 2022
Accepted manuscript online: February 10, 2022
Version of record online: February 28, 2022